The Atmospheric Bridge Communicated the δ¹³C Decline during the Last Deglaciation to the Global Upper Ocean

Jun Shao[1], Lowell D. Stott[1], Laurie Menviel[2], Andy Ridgwell[3], Malin Ödalen[4,5], Mayhar Mohtadi[6]

[1]Department of Earth Science, University of Southern California, Los Angeles, CA 90089, USA

[2]Climate Change Research Centre and PANGEA, University of New South Wales, NSW 2052, Sydney

[3]Department of Earth Sciences, University of California, Riverside, CA 92521, USA

[4]Department of Meteorology, Bolin Centre for Climate Research, Stockholm University, 106 91 Stockholm, Sweden

[5]Department of Geosciences, University of Arizona, Tucson, AZ 85721, USA

[6]MARUM-Center for Marine Environmental Sciences, University of Bremen, 28359 Germany

Correspondence to: Jun Shao (junshao@usc.edu)

Abstract. During the early last glacial termination (17.2-15 ka) atmospheric δ¹³C declined sharply by 0.3-0.4‰ as atmospheric pCO_2 rose. This was the initial part of the atmospheric δ¹³C excursion that lasted for multiple thousand years. A similar δ¹³C decline has been documented in marine proxy records from both surface and thermocline-dwelling planktic foraminifera. The foraminiferal δ¹³C decline has previously been attributed to a flux of respired carbon from the deep ocean that was subsequently transported within the upper ocean (i.e. 'bottom up' transport) to sites where the signal is recorded. Here, we provide modeling evidence that when respired carbon upwells in the Southern Ocean, negative δ¹³C anomalies in the global upper ocean were instead transferred from the atmosphere (i.e. top down transport). Due to this efficient 'atmospheric bridge', the pathway of δ¹³C transport was likely to be different from nutrient transport during the early deglaciation. This implies that the usage of planktic δ¹³C records for identifying the carbon source(s) responsible for the atmospheric pCO_2 rise during the early deglaciation is limited. The model results also suggest that thermocline waters in upwelling systems like the eastern equatorial Pacific, and even upper deep waters above 2000m, can be affected by this atmospheric bridge during the early deglaciation. Our results imply that caution must be applied when interpreting early deglacial marine δ¹³C records from depths that are potentially affected by the atmosphere.

1 Introduction

Atmospheric pCO_2 increased by 80-100 ppm from the last glacial maximum (LGM) to the Holocene (Marcott et al., 2014; Monnin et al., 2001). The mechanisms and the chain of events that were responsible for this pCO_2 rise are not well understood. High resolution ice core CO_2 and $\delta^{13}C$ records provide valuable constraints on the timing and magnitude of this

30   deglacial history. During the initial ~35ppm rise in pCO_2 rise between 17.2 to 15 ka, ice core records have documented a 0.3‰ decrease in atmospheric $\delta^{13}C$ (Bauska et al., 2016; Schmitt et al., 2012). This millennial-scale trend was punctuated by a rapid 12ppm pCO_2 increase between 16.3-16.1 ka (Marcott et al., 2014) and a -0.2‰ decrease in atmospheric $\delta^{13}C$ (Bauska et al., 2016). A contemporaneous $\delta^{13}C$ drop is recorded by both surface and thermocline dwelling foraminifers (e.g. Hertzberg et al., 2016; Lund et al., 2019; Spero & Lea, 2002) as well as by benthic foraminifera from shallow depths (e.g. Lynch-Stieglitz

35   et al., 2019; Romahn et al., 2014; Stott et al., 2019; this study) around the global ocean. The planktic $\delta^{13}C$ records have been previously interpreted to reflect a spread of high nutrient, low $\delta^{13}C$ waters that upwelled in the Southern Ocean, and then transported throughout the upper ocean via a so-called intermediate water teleconnection (Martínez-Botí et al., 2015; Pena et al., 2013; Spero & Lea, 2002). According to this hypothesis, formerly sequestered carbon from deep waters were upwelled in the Southern Ocean (Anderson et al., 2009) in response to a breakdown of deep ocean stratification (Basak et al., 2018) and

40   this carbon was then carried by Antarctic Intermediate Water (AAIW) and Southern Ocean Mode Water (SAMW) to low latitudes where it then outgassed to the atmosphere in upwelling regions like the eastern equatorial Pacific (EEP). This hypothesis implies that the upper ocean at lower latitudes acts as a conduit for ^{13}C-depleted carbon to the atmosphere. Here we term this scenario 'bottom up' transport.

Recently, it has been suggested that a negative $\delta^{13}C$ decline occurring initially in the atmosphere (i.e. as recorded by

45   the ice cores) may have left an isotopic imprint on the global surface ocean through air-sea exchange (Lynch-Stieglitz et al., 2019) . That signal could then be transmitted to thermocline depths and maybe even reach intermediate depths. Here we term this alternative scenario 'top down' transport.

The two scenarios have different implications. In the 'bottom up' transport scenario, a significant portion of ^{13}C-depleted carbon from the deep ocean was outgassed at low latitudes and contributed to the atmospheric pCO_2 rise, while in the

50   'top down' transport, ^{13}C-depleted carbon from the ocean could be outgassed to the atmosphere from anywhere (e.g. the high

latitude Southern Ocean and low latitude upwelling regions), and the subsequent $\delta^{13}C$ decline in the global upper ocean does not necessarily contribute to atmospheric pCO$_2$ variability.

Here, we analyze a transient deglacial simulation conducted with the Earth system model LOVECLIM (Menviel et al., 2018). In this experiment, sequestered respired carbon in the deep and intermediate waters are ventilated through the

55   Southern Ocean and this leads to a sharp decline in atmospheric $\delta^{13}C$, consistent with ice core records. We evaluate the two $\delta^{13}C$ transport scenarios by partitioning the simulated carbon pool and its stable isotope signature into a preformed and a remineralized component (Methods). The preformed component is dominated by surface processes such as air-sea thermodynamic equilibrium and primary productivity. The remineralized component reflects gain/loss of respired carbon due to changes in residence time and export productivity, or a transient input of respired carbon from the deep ocean. If the 'top

60   down' transport scenario was the mechanism responsible for the $\delta^{13}C$ decline seen in marine proxy records, the preformed signal should dominate in the upper 1000m, while a remineralized signal would dominate the 'bottom up' scenario. Our approach requires an accurate representation of the preformed and remineralized component. The LOVECLIM transient experiment does not simulate preformed or remineralized carbon explicitly and our offline calculation (see Methods) is likely subject to errors. However, the LOVECLIM results are complemented by sensitivity experiments performed with another

65   Earth System model (cGENIE), wherein the preformed tracers are explicitly simulated.

The partitioning framework is not new, previous studies have used this framework to study the mechanisms that lead to lower glacial atmospheric CO$_2$ (Ito & Follows, 2005; Khatiwala et al., 2019) and processes that control atmospheric and marine $\delta^{13}C$ (Menviel et al., 2015; Schmittner et al., 2013). This diagnostic framework has also been applied to study the carbon cycle perturbation in response to a weaker AMOC (Schmittner & Lund, 2015), however in that study the experiments

70   were performed under constant pre-industrial conditions. To our knowledge, the origin of the early deglacial $\delta^{13}C$ perturbation has not been established.

We also present a new benthic $\delta^{13}C$ record from the upper western equatorial Pacific (WEP) to expand the deglacial benthic $\delta^{13}C$ dataset of the upper ocean isotope excursion (e.g. Lynch-Stieglitz et al., 2019).

2 Methods

75   **2.1 LOVECLIM deglacial transient simulation**

The LOVECLIM model (Goosse et al., 2010) consists of a free-surface primitive equation ocean model (3° × 3°, 20 vertical

levels), a dynamic–thermodynamic sea ice model, an atmospheric model based on quasi-geostrophic equations of motion (T21,

three vertical levels), a land surface scheme, a dynamic global vegetation model (Brovkin et al., 1997) and a marine carbon

cycle model (Menviel et al., 2015). To study the sensitivity of the carbon cycle to different changes in oceanic circulation, a

80   series of transient simulations of the early part of the last deglaciation (19-15ka) was performed by forcing LOVECLIM with

changes in orbital parameters (Berger, 1978) as well as Northern Hemispheric ice-sheet geometry and albedo (Abe-Ouchi et

al., 2007), and starting from a LGM simulation that best fit oceanic carbon isotopic (^{13}C and ^{14}C) records (Menviel et al., 2017).

The simulation we analyzed for this study is "LH1-SO-SHW" from Menviel et al, (2018). We briefly describe the relevant

deglacial forcing here. Firstly, a freshwater flux of 0.07 Sv is added into the North Atlantic between 17.6 ka and 16.2 ka,

85   resulting in an AMOC shut down. Secondly, a salt flux is added into the Southern Ocean between 17.2 ka and 16.0 ka to

enhance Antarctic Bottom Water (AABW) formation. Enhanced AABW could have occurred due to changes in buoyancy

forcing at the surface of the Southern Ocean, or opening of polynyas, processes which could be mis-represented in the model

due to its relatively coarse resolution. Lastly, two stages of enhanced Southern Ocean westerlies are prescribed in the

simulation at 17.2 ka and at 16.2 ka; this timing generally corresponds to Southern Ocean warming associated with two phases

90   of NADW weakening during Heinrich Stadial 1 (Hodell et al., 2017). For more detail about this experiment, see Menviel et

al., (2018).

2.2 cGENIE Sensitivity experiments

The cGENIE model is also based on a 3-D dynamical ocean model plus dynamic and thermodynamic sea ice

components but run at a lower resolution (36x36 horizontal grid with 16 vertical layers.) than LOVECLIM. In addition,

95   cGENIE lacks a dynamical atmosphere. Climate feedback is instead provided by a 2-D energy-moisture balance atmosphere

(Edwards & Marsh, 2005), making it much less computationally expensive than LOVECLIM. cGENIE includes a

representation of marine biogeochemical cycling (Ridgwell et al., 2007). Preformed dissolved inorganic carbon (DIC$_{pref}$) and

δ^{13}C (δ^{13}C$_{pref}$) tracers are explicitly simulated in cGENIE (Ödalen et al., 2018). These are created by resetting the preformed

tracer value at the ocean surface to the equivalent full tracer value at each model time-step, and then allowing ocean circulation

100   to transport the preformed tracers conservatively – i.e. no remineralization or other interior ocean geochemical processes are

allowed to modify the preformed tracer value.

A series of cGENIE simulations were run based on the pre-industrial configuration of Cao et al., (2009) (Table 1). The spin-up includes two stages: the first stage was run for 10,000 years, with prescribed atmospheric $pCO_2 = 278$ ppm, $\delta^{13}C$ = -6.5‰; the second stage was run for 3,000 years, with a 0.1 Sv of freshwater input into the North Atlantic to weaken the

105   Atlantic Meridional Overturning Circulation (AMOC). The atmosphere is fixed at the first stage. We then performed 2 idealized simulations to investigate the role of air-sea exchange in upper ocean $\delta^{13}C$, each integrated for 2000 years. In these sensitivity experiments, in addition to a continuous freshwater flux into the North Atlantic, we applied a -0.3 Sv freshwater flux (i.e. salt flux) into the Pacific sector of the surface Southern Ocean to enhance AABW formation and ventilation rate. In the experiment 'fix', the atmosphere is held constant as in the spin up. In the experiment 'free', the atmosphere is allowed to

110   evolve freely. The radiative forcing for both experiments is fixed at the pre-industrial level so that the two experiments have an identical climate even though the CO_2 concentrations will differ. Note also that by holding the atmospheric CO_2 and $\delta^{13}C$ constant in the experiment 'fix', the atmosphere-ocean inventories of carbon and $\delta^{13}C$ are slightly different from those in the experiment 'free'.

2.3 Carbon pool partitioning

115

To diagnose the mechanisms responsible for the carbon isotope perturbation, the DIC pool is separated into remineralized and preformed components: $DIC = DIC_{reg} + DIC_{pref}$ (Ito & Follows, 2005). DIC_{reg} consists of remineralized organic matter (DIC_{org}) and remineralized calcium carbonate (DIC_{CaCO3}). In LOVECLIM, DIC_{org} is estimated by the Apparent Oxygen Utilization (AOU); AOU is the difference between saturation concentration for oxygen at the ambient temperature

120   and salinity and in situ oxygen. $DIC_{org} = -R_{C/O} * AOU$, where $R_{C/O} = 117:-170$ (Anderson & Sarmiento, 1994). DIC_{org} is highly depleted in $\delta^{13}C$ and changes in DIC_{org} has a strong impact on the $\delta^{13}C$ budget. DIC_{CaCO3}, on the other hand, has an isotopic composition close to seawater and does not have a strong influence on oceanic $\delta^{13}C$ variability. DIC_{CaCO3} and its impact on $\delta^{13}C$ is therefore not considered in this study. Changes in $\delta^{13}C$ ($\Delta\delta^{13}C$) due to remineralization of organic matter is estimated by $\Delta\delta^{13}C_{reg} = \delta^{13}C_{org} * \Delta(^{12}C_{org} / ^{12}C) = \delta^{13}C_{org} * \Delta(^{12}C_{org}/DIC)$; $\Delta\delta^{13}C$ in response to perturbations of the preformed pool

125   ($\Delta\delta^{13}C_{pref}$) is estimated by $\Delta\delta^{13}C$ - $\Delta\delta^{13}C_{reg}$.

In cGENIE, $\delta^{13}C_{pref}$ is explicitly simulated and the remineralization effect is estimated by $\Delta\delta^{13}C_{reg}= \Delta\delta^{13}C- \Delta\delta^{13}C_{pref}$.

2.4 Stable Isotope Analyses and Age Model for Piston Core GeoB17402

The WEP piston core GeoB17402 (8°N, 126°34'E, 556m) was recovered from the expedition SO-228. The planktic

foraminiferal samples for ^{14}C age dating were typically between 2 and 5mg. All new radiocarbon ages were measured at the

130   University of California Irvine Accelerator laboratory. An age model was developed for this core by converting the *Trilobatus*

sacculifer (*T. sacculifer*)^{14}C ages to calendar age using BChron and the Marine13 calibration database. There is no evidence

that surface reservoir ages were significantly different during the glacial or deglacial period. We therefore did not apply any

adjustment to Delta R. Once the calendar ages were established the results were plotted vs depth. Between each adjacent *T.*

sacculifer age, linear interpolation was applied to develop an age model for the core. For benthic foraminiferal $\delta^{18}O$ and $\delta^{13}C$

135   measurements approximately 4-8 *Cibicidoides mundulus* (*C. mundulus*) were picked. These samples were cleaned by first

cracking the tests open and then sonicating them in deionized water after which they were dried at low temperature. The isotope

measurements were conducted at the University of Southern California on a GV Instruments Isoprime mass spectrometer

equipped with an autocarb device. An in-house calcite standard (ultissima marble) was run in conjunction with foraminiferal

samples to monitor analytical precision. The 1σ standard deviation for standards measured during the study was less than 0.1‰

140   for both $\delta^{18}O$ and $\delta^{13}C$. The stable isotope data are reported in per mil with respect to VPDB and will be archived on Pangaea.

3 Results

In the LOVECLIM transient simulation, freshwater input into the North Atlantic leads to reduced North Atlantic

Deep Water (NADW) formation. Atlantic Meridional Overturning Circulation (AMOC) is significantly weaker than its glacial

145   condition by ~18 ka (Figure 1a), but this only has a minor effect on the atmospheric CO_2 (Figure 1b) and $\delta^{13}C$ (Figure 1c). On

the other hand, enhanced ventilation of Antarctic bottom water (AABW) and Antarctic intermediate water (AAIW) between

17.2-15 ka leads to an atmospheric CO_2 increase of ~25 ppm and $\delta^{13}C$ decline of -0.35‰ (Figure 1b, 1c). Below, our analyses

center around the Pacific basin between 17.2 - 15.0 ka. The Atlantic basin will be discussed in Sect. 4.3.

The model simulates a global negative sea surface $\delta^{13}C$ anomaly (here defined as 15-17.2 ka) (Figure 2a). The

150   strongest negative anomaly occurs at the surface of the Southern Ocean and North Atlantic. We separate the simulated sea

surface $\delta^{13}C$ signal (Figure 2a) into 2 components: 1) air-sea thermodynamic component due to atmospheric $\delta^{13}C$ and sea

surface temperature (SST) changes ($\Delta\delta^{13}C_{thermo}$, Figure 2b) (Zhang et al., 1995) (Note the SST effect ($\Delta\delta^{13}C_{sst}$) alone is shown

in figure S2.) and 2) the residual component ($\Delta\delta^{13}C_{res}$) (Figure 2c) that mainly reflects enhanced primary productivity in

response to increased nutrient supply upwelled from the deep ocean (Figure S3). The surface $\Delta\delta^{13}C$ (Figure 2a) is then

155   propagated into the ocean interior as a preformed signal when surface waters subduct. To the North of 50°S in the Pacific, $\delta^{13}C$

in the upper 1000m (Figure 3a) is dominated by a preformed signal of ~-0.3‰ (Figure 3c), with minor contribution from

respired carbon transport within the ocean interior (Figure 3b).

In the Pacific, $\Delta\delta^{13}C_{pref}$ of -0.2 to -0.3‰ can be traced to ~1000 m in the LOVECLIM simulation (Figure 3c). Since

there is a minor change in $\Delta\delta^{13}C_{reg}$ above 1000m in the tropical Pacific, this preformed signal would have been recorded by

160   benthic foraminifera from this region. Indeed, our new record from 556 m depth in the WEP (Figure 4b) documents a -0.3 to

-0.4‰ decline during the early deglaciation (Figure 4b), consistent with records from the EEP at similar depths (Stott et al.,

2019). We acknowledge that the magnitude of increasing $\delta^{13}C$ between 15-13 ka is much larger in our benthic $\delta^{13}C$ record,

which might be caused by other factors. Nonetheless, our new shallow benthic $\delta^{13}C$ records share a similar 'W' shape as the

atmospheric record over the last 20ka, suggesting a sustained influence from the atmosphere.

165   Our results support the 'top down' transport scenario and challenges the 'bottom up' transport scenario as the primary

mechanism for the $\delta^{13}C$ decline seen in upper ocean proxy reconstructions. The 'top down' scenario is also compatible with

the idea of a nutrient teleconnection between the Southern Ocean and low latitudes (Palter et al., 2010; Pasquier & Holzer,

2016; Sarmiento et al., 2004). Figure 3d illustrates that stronger upwelling brings excess nutrients to the surface of the Southern

Ocean. Unused nutrients are then transported to low latitudes within the upper ocean circulation (e.g. through mode waters

170   and thermocline waters). However, a nutrient teleconnection does not, in itself, reflect enhanced flux of $\delta^{13}C$-depleted DIC

from the deep ocean to low latitudes in a 'tunnel-like' fashion. The $\delta^{13}C$ signal that is transported in the upper ocean has been

strongly affected by air-sea gas exchange at the surface of Southern Ocean and therefore its pathway is different from the

nutrient signal in the LOVECLIM simulation.

To be clear, the stronger negative $\Delta\delta^{13}C_{pref}$ compared to $\Delta\delta^{13}C_{reg}$ in the upper ocean does not mean respired carbon is

175   not important in the simulation. In fact, the ultimate δ^{13}C-depleted carbon source in LOVECLIM is the simulated respired

carbon that accumulated in the deep and intermediate waters during the glacial period as a consequence of the imposed

weakened deep water formation. Our results suggest that when deep ocean stratification breaks down in the model, the δ^{13}C-

depleted deep waters upwell; the signal is transmitted to the atmosphere through strong outgassing in the Southern Ocean

(Figure 5). Subsequently, equilibrium thermodynamic exchange between the atmosphere and the surface ocean dominates the

180   δ^{13}C decline in the global upper ocean.

Our approach to partitioning carbon in LOVECLIM is not perfect and subject to errors. For example, AOU likely

over estimates the true Oxygen Utilization, and thus DIC_{org}, particularly in water masses formed in regions with sea ice

(Bernardello et al., 2014; Ito et al., 2004; Khatiwala et al., 2019). To confirm the results obtained from the LOVECLIM

simulation are robust, we conducted experiments with another Earth System model – cGENIE. In cGENIE, similar

185   freshwater/salt forcing as in the LOVECLIM simulation were applied. Unlike LOVECLIM, in cGENIE carbon partitioning

can be performed in a traceable and more accurate manner (see Methods). In the cGENIE 'free' experiment, enhanced deep

ocean ventilation is associated with a rapid decrease in upper ocean δ^{13}C during the first 1000 years and then stabilizes between

model year 1000 and 2000 (not shown). The δ^{13}C decline in the upper 1000m is also dominated by the preformed signal (Figure

6), consistent with the LOVECLIM simulation. When atmospheric pCO$_2$ and atmospheric δ^{13}C are held constant in experiment

190   'fix', the $\Delta\delta^{13}C_{pref}$ in the upper 500m is very small (Figure 6d). These sensitivity experiments with cGENIE further reinforce

the fact that it is the atmospheric signal that dominates the upper ocean δ^{13}C response.

We acknowledge that LOVECLIM and cGENIE are two distinct models and initial conditions, boundary conditions,

prescribed forcing in the simulations are all quite different. For example, the LOVECLIM simulation starts with a glacial like

climate and a strong stratified deep ocean; atmospheric pCO$_2$ increases from 190 ppm to 207 ppm between 17.2 ka and 15 ka.

195   The cGENIE simulations begin with a pre-industrial like climate; atmospheric pCO$_2$ increases from 278 ppm to 310 ppm.

Thus, direct comparisons between the model simulations are not our focus. Nonetheless, both models suggest upper ocean

δ^{13}C cannot be used as a direct tracer of respired carbon transport during the deglaciation, due to the influence of air-sea

exchange.

4 Discussion:

4.1 Atmospheric δ¹³C Bridge

Our simulations imply that the wide-spread deglacial δ¹³C minimum observed in marine planktic records can be explained, to the first order, by air-sea gas exchange (Lynch-Stieglitz et al., 2019) originating from the atmosphere. The atmosphere seems to act as a bridge in transmitting a lower δ¹³C signal from sites where δ¹³C-depleted carbon is released to the atmosphere (i.e. high latitude Southern Ocean in the LOVECLIM and cGENIE simulation) into the global surface and subsurface ocean. A good example is the simulated transient δ¹³C minimum event between 16.2 -15.8 ka in LOVECLIM (Figure 1c), which clearly originates from the Southern Hemisphere and particularly from enhanced ventilation of AAIW (Figure 1a). If the 'top down' scenario is true, the upper water masses away from the Southern Hemisphere would show similar magnitude of δ¹³C changes as the atmosphere, while water masses in the mid or high latitude Southern Hemisphere may show different δ¹³C responses due to dynamical circulation and productivity changes induced by Southern Ocean processes. On the other hand, if the 'bottom up' scenario is true, a large depleted δ¹³C signal should first appear in the South Pacific subtropical gyre (STGSP), then progressively spread to the tropics and finally reach the North Pacific; the depleted δ¹³C anomaly is also likely to be diluted along its pathway from the South Pacific to the North Pacific. In the LOVECLIM simulation, there is no δ¹³C minimum in the upstream STGSP, while the atmosphere-like negative δ¹³C anomaly appears in the EEP thermocline, the North Pacific subtropical gyre (STGNP) and North Pacific Intermediate Water (NPIW) simultaneously (Figure 7). In addition, millennial-scale δ¹³C evolution in these upper ocean water masses to the north of the equator all show pattern similar to the atmosphere. The synchronized δ¹³C anomaly clearly points to the dominant role of atmospheric communication rather than time-progressive oceanic transport of a low δ¹³C signal in LOVECLIM.

In the LOVECLIM simulation, both millennial- and centennial-scale atmospheric δ¹³C declines are the result of enhanced deep ocean and/or intermediate ocean ventilation through the Southern Ocean. Using the UVic Earth-System model, Schmittner and Lund (2015) showed that a slow-down of AMOC alone is able to weaken the global biological pump and lead to light carbon accumulation in the upper ocean and the atmosphere, without invoking any Southern Ocean processes. Despite the different prescribed forcing, $\Delta\delta^{13}C_{pref}$ also dominates the total $\Delta\delta^{13}C$ in the upper 1000m of the global ocean in the UVic

experiment (See fig. 6 in Schmittner & Lund, 2015). Taken together, simulations by all three models suggest that any process

225   that lowers the atmospheric $\delta^{13}C$ would have an influence on the global upper ocean $\delta^{13}C$. This limits the use of planktic $\delta^{13}C$

records alone for identifying source(s) and locations of light carbon released to the atmosphere during the last deglaciation,

consistent with what Lynch-Stieglitz et al., (2019) proposed. In section 4.2 and 4.3, we provide two examples over the last

deglaciation to illustrate how recognizing the role of 'atmospheric bridge' in transmitting $\delta^{13}C$ anomaly could lead to critical

re-evaluation of what marine $\delta^{13}C$ records actually reveal. Ice core records have documented multiple atmospheric $\delta^{13}C$

230   excursions during the last glacial period (Eggleston et al., 2016), our findings thus have important implications for interpreting

marine $\delta^{13}C$ records over glacial cycles.

4.2 Revisiting EEP Thermocline $\delta^{13}C$

Waters at eastern equatorial Pacific (EEP) thermocline depths are thought to be connected to the deep ocean through

AAIW from the south and NPIW from the north. The EEP is therefore a potential conduit for deep ocean carbon release to the

235   atmosphere. As illustrated in the result section, the LOVECLIM simulated $\delta^{13}C$ changes in the thermocline of the EEP mainly

reflects a preformed signal. In the cGENIE experiment 'free', $\Delta\delta^{13}C_{pref}$ also plays a dominant role in the total $\Delta\delta^{13}C$ signal in

the thermocline EEP. In contrast, in the experiment 'fix', there is almost no change in $\delta^{13}C$ (Table 2). Thus, the release of

isotopically-light carbon through the surface Southern Ocean (in both exp 'fix' and 'free') and the consequential air-sea re-

equilibration of $\delta^{13}C$ through gas exchange (in exp 'free' only) are both necessary to obtain the observed magnitude of $\delta^{13}C$

240   decline within the EEP thermocline.

The EEP is a dynamical region and observed $\delta^{13}C$ variability in its upper waters likely reflects local processes that

are not accounted for by the LOVECLIM simulation. However, we would like to highlight two planktic $\delta^{13}C$ records that show

strikingly similar evolution to the model simulation (Figure 8, Figure S4). Site GGC17/JPC30 is close to the coast and the

wood-constrained constant surface reservoir ages over the last 20ka suggest this site was not influenced by old respired carbon

245   from high latitudes (Zhao & Keigwin, 2018). Site ODP1238 is located in the main upwelling region where strengthened CO_2

outgassing inferred from boron isotope data has been interpreted to reflect respired carbon transported from the Southern

Ocean (Martínez-Botí et al., 2015). If the deglacial history of subsurface influence was indeed distinctively different at the two

sites, the remarkably similar planktic $\delta^{13}C$ evolution provides strong evidence that thermocline $\delta^{13}C$ in the EEP is dominantly

controlled by the 'top down' mechanism rather than the 'bottom up' mechanism as previously suggested (Martínez-Botí et al.,

250   2015; Spero & Lea, 2002), consistent with the LOVECLIM simulation (Figure 8). At the same time, if there was significant

outgassing in the EEP as expressed in the Boron isotope results (Martínez-Botí et al., 2015), the EEP itself could have partially

contributed to the overall deglacial atmospheric $\delta^{13}C$ evolution that dominates upper ocean $\delta^{13}C$ response.

Collectively, our results show that even in strong upwelling regions, where atmospheric $\delta^{13}C$ signal from above are

likely to be erased by outcropping subsurface waters from below, thermocline $\delta^{13}C$ is still subjected to strong atmosphere

255   influences. This implies that the upper few hundred meters of the water column can be influenced by the atmosphere, consistent

with our interpretation of the new benthic $\delta^{13}C$ record presented in this study.

4.3 How deep can the low preformed $\delta^{13}C$ signal reach during the early deglaciation?

We have shown that given the dominant negative $\delta^{13}C_{pref}$ anomaly in the upper ocean, some interpretation of planktic

260    $\delta^{13}C$ records might need to be re-evaluated. Our simulations also reveal that an atmospheric influence can reach deeper than

thermocline depths, which is supported by the fact that some benthic $\delta^{13}C$ records from upper 1000m resemble the atmospheric

$\delta^{13}C$ evolution. It is plausible that below 1000m, a $\Delta\delta^{13}C_{pref}$ signal from the atmosphere still exists, but no longer dominates

the total $\Delta\delta^{13}C$ as $\Delta\delta^{13}C_{reg}$ becomes increasingly important at depth.

It has been suggested that deglacial $\delta^{13}C$ variability in the waters above 2000m depth in the Atlantic could be driven

265   by air-sea exchange (Lynch-Stieglitz et al., 2019). However, mid-depth (1800-2100m) benthic $\delta^{13}C$ records from the Brazil

margin (~27°S) document a $\delta^{13}C$ decline of -0.4‰ between 18.3 and 17 ka, earlier than the atmospheric $\delta^{13}C$ signal, which

decreases between 17 and 15 ka (Lund et al., 2019). Lund et al., (2019) suggest these observations seem at odds with the idea

that $\delta^{13}C_{pref}$ contributed to $\delta^{13}C$ variability at their site.

The observed benthic $\delta^{13}C$ anomaly at these Brazil margin sites are well simulated by LOVECLIM (Figure 9). Prior

270   to 17.2 ka, $\delta^{13}C$ variability at ~2000m depth at the Brazil Margin in the LOVECLIM simulation is dominantly controlled by

accumulation of respired carbon (Figure S5b) and there is only a minor contribution from $\delta^{13}C_{pref}$ (Figure S5c), as previous

studies suggested (Lacerra et al., 2017; Lund et al., 2019; Schmittner & Lund, 2015). Interestingly, LOVECLIM also reveals

a strong negative $\Delta\delta^{13}C_{pref}$ signal between 17-15ka when the atmospheric $\delta^{13}C$ declines (Figure 10c). But a positive $\Delta\delta^{13}C_{reg}$

(Figure 10b) signal originating from a loss of respired carbon due to enhanced ventilation at those depths completely

275   compensates for the negative $\Delta\delta^{13}C_{pref}$. As a result, there is only a minor $\Delta\delta^{13}C$ (Figure 10a) signal, which is consistent with

the proxy observations.

It is not clear why the simulated $\Delta\delta^{13}C_{pref}$ values are more negative in the Atlantic than in the Pacific in LOVECLIM

simulation (compare figure 3c and Figure 10c). It could be due to different circulation and/or subduction of different water

masses in the two basins. Nonetheless, these results suggest that, between 17.2 and 15ka, a negative preformed $\delta^{13}C$ signal

280   from the atmosphere needs to be considered when interpreting benthic $\delta^{13}C$ records shallower than 2000m depth.

5 Conclusions:

The LOVECLIM transient simulation is used as a tool to investigate the pathway of low $\delta^{13}C$ signal transport under

a prevailing deglacial scenario that involves Southern Ocean processes. We have shown that ocean-atmosphere gas exchange

285   likely dominates the negative $\delta^{13}C$ anomalies documented in surface and upper ocean proxy reconstructions between 17.2 ka

and 15 ka. Numerical simulations suggest that enhanced Southern Ocean upwelling leads to a transfer of $\delta^{13}C$-depleted respired

carbon from the Southern Ocean directly to the atmosphere. Consequently, atmospheric $\delta^{13}C$ declines and this leaves its imprint

on the global upper ocean through air-sea equilibration. This preformed signal could account for a marine $\delta^{13}C$ decline up to

0.3-0.4‰ at the surface and down to 2000m depth during the early deglaciation. At the same time, the amount of upwelling in

290   the Southern Ocean is a forcing imposed on the model and therefore it is not directly constrained. It is therefore possible there

were other sites where excess carbon was ventilated to the atmosphere during the deglaciation, which would have also affected

atmospheric $\delta^{13}C$. Our findings therefore imply that planktic $\delta^{13}C$ records do not provide strong constraints on the site or the

mechanisms through which CO_2 was released from the ocean to the atmosphere. Interpretation of early deglacial benthic $\delta^{13}C$

records shallower than 2000m depth needs to take into account an atmospheric influence. Whereas in the model simulations

295   the source of the atmospheric signal is a direct response to enhanced Southern Ocean upwelling, our results underscore the

need to find a way to fingerprint the actual source(s) of ^{13}C-depleted carbon that caused the atmospheric $\delta^{13}C$ decline.

300

Data availability. All data generated or analysed during this study can be made available upon request to the corresponding author (J.S.).

Author contribution. J.S designed the research with input from L.S. L.M provided the LOVECLIM output. J.S. performed

305 the cGENIE simulations with help from A.R. J.S, L.M. and M.Ö analyzed the model simulations. M.M was the chief scientist of the SO-228 expedition and provided samples from the GeoB 17402 core. J.S. wrote the manuscript with contributions from all co-authors.

Competing interests. The authors declare that they have no conflict of interest.

310

Acknowledgements. This work is supported by the National Science Foundation under Grant Numbers 1558990 (to J.S. and L.S.) and 1736771 (A.R.). L.M. acknowledges funding from the Australian Research Council grants FT180100606 and DP180100048. A.R. acknowledges funding from the Heising Simons Foundation. M.Ö acknowledges the Bolin Centre for Climate Research for support. The funding for the expedition SO-228 is from BMBF (German Ministry of

315 Education and Research) grant #03G0228A.

320

References:

325 Abe-Ouchi, A., Segawa, T., & Saito, F. (2007). Climatic Conditions for modelling the Northern Hemisphere ice sheets
throughout the ice age cycle. *Clim. Past*, 16.

Anderson, L. A., & Sarmiento, J. L. (1994). Redfield ratios of remineralization determined by nutrient data analysis. *Global
Biogeochemical Cycles*, *8*(1), 65–80. https://doi.org/10.1029/93GB03318

Anderson, R. F., Ali, S., Bradtmiller, L. I., Nielsen, S. H. H., Fleisher, M. Q., Anderson, B. E., & Burckle, L. H. (2009).

330   Wind-Driven Upwelling in the Southern Ocean and the Deglacial Rise in Atmospheric CO_2. *Science*, *323*(5920),
1443–1448. https://doi.org/10.1126/science.1167441

Basak, C., Fröllje, H., Lamy, F., Gersonde, R., Benz, V., Anderson, R. F., et al. (2018). Breakup of last glacial deep
stratification in the South Pacific. *Science*, *359*(6378), 900–904. https://doi.org/10.1126/science.aao2473

Bauska, T. K., Baggenstos, D., Brook, E. J., Mix, A. C., Marcott, S. A., Petrenko, V. V., et al. (2016). Carbon isotopes

335   characterize rapid changes in atmospheric carbon dioxide during the last deglaciation. *Proceedings of the National
Academy of Sciences*, *113*(13), 3465–3470. https://doi.org/10.1073/pnas.1513868113

Bereiter, B., Eggleston, S., Schmitt, J., Nehrbass-Ahles, C., Stocker, T. F., Fischer, H., et al. (2015). Revision of the EPICA
Dome C CO_2 record from 800 to 600 kyr before present: Analytical bias in the EDC CO_2 record. *Geophysical
Research Letters*, *42*(2), 542–549. https://doi.org/10.1002/2014GL061957

340 Berger, AndréL. (1978). Long-Term Variations of Daily Insolation and Quaternary Climatic Changes. *Journal of the
Atmospheric Sciences*, *35*(12), 2362–2367. https://doi.org/10.1175/1520-0469(1978)035<2362:LTVODI>2.0.CO;2

Bernardello, R., Marinov, I., Palter, J. B., Sarmiento, J. L., Galbraith, E. D., & Slater, R. D. (2014). Response of the Ocean
Natural Carbon Storage to Projected Twenty-First-Century Climate Change. *Journal of Climate*, *27*(5), 2033–2053.
https://doi.org/10.1175/JCLI-D-13-00343.1

345 Brovkin, V., Ganopolski, A., & Svirezhev, Y. (1997). A continuous climate-vegetation classification for use in climate-
biosphere studies. *Ecological Modelling*, *101*(2–3), 251–261. https://doi.org/10.1016/S0304-3800(97)00049-5

Cao, L., Eby, M., Ridgwell, A., Caldeira, K., Archer, D., Ishida, A., et al. (2009). The role of ocean transport in the uptake of
anthropogenic CO_2. *Biogeosciences*, *6*(3), 375–390. https://doi.org/10.5194/bg-6-375-2009

Edwards, N. R., & Marsh, R. (2005). Uncertainties due to transport-parameter sensitivity in an efficient 3-D ocean-climate

350   model. *Climate Dynamics*, *24*(4), 415–433. https://doi.org/10.1007/s00382-004-0508-8

Eggleston, S., Schmitt, J., Bereiter, B., Schneider, R., & Fischer, H. (2016). Evolution of the stable carbon isotope

composition of atmospheric CO $_2$ over the last glacial cycle: δ ^{13} C(ATM) OVER THE LAST GLACIAL CYCLE.

Paleoceanography, *31*(3), 434–452. https://doi.org/10.1002/2015PA002874

Goosse, H., Brovkin, V., Fichefet, T., Haarsma, R., Huybrechts, P., Jongma, J., et al. (2010). Description of the Earth system

355   model of intermediate complexity LOVECLIM version 1.2. *Geoscientific Model Development*, *3*(2), 603–633.

https://doi.org/10.5194/gmd-3-603-2010

Hertzberg, J. E., Lund, D. C., Schmittner, A., & Skrivanek, A. L. (2016). Evidence for a biological pump driver of

atmospheric CO $_2$ rise during Heinrich Stadial 1: Bio Pump and CO $_2$ Rise During HS1. *Geophysical Research

Letters*, *43*(23), 12,242-12,251. https://doi.org/10.1002/2016GL070723

360   Hodell, D. A., Nicholl, J. A., Bontognali, T. R. R., Danino, S., Dorador, J., Dowdeswell, J. A., et al. (2017). Anatomy of

Heinrich Layer 1 and its role in the last deglaciation: HEINRICH EVENT 1. *Paleoceanography*, *32*(3), 284–303.

https://doi.org/10.1002/2016PA003028

Ito, T., Follows, M. J., & Boyle, E. A. (2004). Is AOU a good measure of respiration in the oceans?: AOU AND

RESPIRATION. *Geophysical Research Letters*, *31*(17), n/a-n/a. https://doi.org/10.1029/2004GL020900

365   Ito, Takamitsu, & Follows, M. J. (2005). Preformed phosphate, soft tissue pump and atmospheric CO₂.

Journal of Marine Research, *63*(4), 813–839. https://doi.org/10.1357/0022240054663231

Khatiwala, S., Schmittner, A., & Muglia, J. (2019). Air-sea disequilibrium enhances ocean carbon storage during glacial

periods. *Science Advances*, *5*(6), eaaw4981. https://doi.org/10.1126/sciadv.aaw4981

Lacerra, M., Lund, D., Yu, J., & Schmittner, A. (2017). Carbon storage in the mid-depth Atlantic during millennial-scale

370   climate events: Mid-depth Atlantic Carbon Storage. *Paleoceanography*, *32*(8), 780–795.

https://doi.org/10.1002/2016PA003081

Lund, D., Hertzberg, J., & Lacerra, M. (2019). Carbon isotope minima in the South Atlantic during the last deglaciation:

evaluating the influence of air-sea gas exchange. *Environmental Research Letters*, *14*(5), 055004.

https://doi.org/10.1088/1748-9326/ab126f

375 Lund, D. C., Tessin, A. C., Hoffman, J. L., & Schmittner, A. (2015). Southwest Atlantic water mass evolution during the last

deglaciation: DEGLACIAL SOUTHWEST ATLANTIC CIRCULATION. *Paleoceanography*, *30*(5), 477–494.

https://doi.org/10.1002/2014PA002657

Lynch-Stieglitz, J., Valley, S. G., & Schmidt, M. W. (2019). Temperature-dependent ocean–atmosphere equilibration of

carbon isotopes in surface and intermediate waters over the deglaciation. *Earth and Planetary Science Letters*, *506*,

380   466–475. https://doi.org/10.1016/j.epsl.2018.11.024

Marcott, S. A., Bauska, T. K., Buizert, C., Steig, E. J., Rosen, J. L., Cuffey, K. M., et al. (2014). Centennial-scale changes in

the global carbon cycle during the last deglaciation. *Nature*, *514*(7524), 616–619.

https://doi.org/10.1038/nature13799

Martínez-Botí, M. A., Marino, G., Foster, G. L., Ziveri, P., Henehan, M. J., Rae, J. W. B., et al. (2015). Boron isotope

385   evidence for oceanic carbon dioxide leakage during the last deglaciation. *Nature*, *518*(7538), 219–222.

https://doi.org/10.1038/nature14155

Menviel, L., Mouchet, A., Meissner, K. J., Joos, F., & England, M. H. (2015). Impact of oceanic circulation changes on

atmospheric $\delta^{13}CO_2$: $\delta^{13}CO_2$. *Global Biogeochemical Cycles*, *29*(11), 1944–1961.

https://doi.org/10.1002/2015GB005207

390 Menviel, L., Spence, P., Yu, J., Chamberlain, M. A., Matear, R. J., Meissner, K. J., & England, M. H. (2018). Southern

Hemisphere westerlies as a driver of the early deglacial atmospheric CO_2 rise. *Nature Communications*, *9*(1).

https://doi.org/10.1038/s41467-018-04876-4

Monnin, E., Indermuhle, A., Dallenbach, A., Fluckiger, J., Stauffer, B., Stocker, T. F., et al. (2001). Atmospheric CO_2

Concentrations over the Last Glacial Termination. *Science*, *291*(5501), 112–114.

395   https://doi.org/10.1126/science.291.5501.112

Ödalen, M., Nycander, J., Oliver, K. I. C., Brodeau, L., & Ridgwell, A. (2018). The influence of the ocean circulation state on ocean carbon storage and CO₂ drawdown potential in an Earth system model. *Biogeosciences*, *15*(5), 1367–1393. https://doi.org/10.5194/bg-15-1367-2018

Palter, J. B., Sarmiento, J. L., Gnanadesikan, A., Simeon, J., & Slater, R. D. (2010). Fueling export production: nutrient
400   return pathways from the deep ocean and their dependence on the Meridional Overturning Circulation. *Biogeosciences*, *7*(11), 3549–3568. https://doi.org/10.5194/bg-7-3549-2010

Pasquier, B., & Holzer, M. (2016). The plumbing of the global biological pump: Efficiency control through leaks, pathways, and time scales: PLUMBING OF THE GLOBAL BIOLOGICAL PUMP. *Journal of Geophysical Research: Oceans*, *121*(8), 6367–6388. https://doi.org/10.1002/2016JC011821

405   Pena, L. D., Goldstein, S. L., Hemming, S. R., Jones, K. M., Calvo, E., Pelejero, C., & Cacho, I. (2013). Rapid changes in meridional advection of Southern Ocean intermediate waters to the tropical Pacific during the last 30kyr. *Earth and Planetary Science Letters*, *368*, 20–32. https://doi.org/10.1016/j.epsl.2013.02.028

Ridgwell, A., Hargreaves, J. C., Edwards, N. R., Annan, J. D., Lenton, T. M., Marsh, R., et al. (2007). Marine geochemical data assimilation in an efficient Earth System Model of global biogeochemical cycling. *Biogeosciences*, *4*(1), 87–
410   104.

Romahn, S., Mackensen, A., Groeneveld, J., & Pätzold, J. (2014). Deglacial intermediate water reorganization: new evidence from the Indian Ocean. *Climate of the Past*, *10*(1), 293–303. https://doi.org/10.5194/cp-10-293-2014

Sarmiento, J. L., Gruber, N., Brzezinski, M. A., & Dunne, J. P. (2004). High-latitude controls of thermocline nutrients and low latitude biological productivity. *Nature*, *427*(6969), 56–60. https://doi.org/10.1038/nature02127

415   Schmitt, J., Schneider, R., Elsig, J., Leuenberger, D., Lourantou, A., Chappellaz, J., et al. (2012). Carbon Isotope Constraints on the Deglacial CO$_2$ Rise from Ice Cores. *Science*, *336*(6082), 711–714. https://doi.org/10.1126/science.1217161

Schmittner, A., & Lund, D. C. (2015). Early deglacial Atlantic overturning decline and its role in atmospheric CO$_2$ rise inferred from carbon isotopes (δ^{13}C). *Climate of the Past*, *11*(2), 135–152. https://doi.org/10.5194/cp-11-135-2015

Schmittner, A., Gruber, N., Mix, A. C., Key, R. M., Tagliabue, A., & Westberry, T. K. (2013). carbon isotope ratios (δ13C)
420   in the ocean, 24.

Spero, H. J. (2002). The Cause of Carbon Isotope Minimum Events on Glacial Terminations. *Science*, *296*(5567), 522–525.

    https://doi.org/10.1126/science.1069401

Spero, Howard J., Mielke, K. M., Kalve, E. M., Lea, D. W., & Pak, D. K. (2003). Multispecies approach to reconstructing

    eastern equatorial Pacific thermocline hydrography during the past 360 kyr: PAST EASTERN EQUATORIAL

425   PACIFIC HYDROGRAPHY. *Paleoceanography*, *18*(1), n/a-n/a. https://doi.org/10.1029/2002PA000814

Stott, L. D., Harazin, K. M., & Quintana Krupinski, N. B. (2019). Hydrothermal carbon release to the ocean and atmosphere

    from the eastern equatorial Pacific during the last glacial termination. *Environmental Research Letters*, *14*(2),

    025007. https://doi.org/10.1088/1748-9326/aafe28

Zhang, J., & Quay, P. D. (n.d.). Carbon isotope fractionation during gas-water exchange and dissolution of CO, 8.

430   Zhao, N., & Keigwin, L. D. (2018). An atmospheric chronology for the glacial-deglacial Eastern Equatorial Pacific. *Nature*

    Communications, *9*(1). https://doi.org/10.1038/s41467-018-05574-x

435

440

445

450

Table 1. Prescribed forcings in cGENIE experiments

	spin	free	fix
NA freshwater flux	+0.1Sv	+0.1Sv	+0.1Sv
SO freshwater flux	0	-0.3 Sv	-0.3Sv
atmosphere	pCO$_2$=278 ppm; δ^{13}C$_{atm}$= -6.5‰	freely evolve	pCO$_2$=278 ppm; δ^{13}C$_{atm}$= -6.5‰

Table 2. δ^{13}C Response in cGENIE experiments. $\Delta\delta^{13}$C is defined as the difference between model year 2000 and 0.

Variable	'free'	'fix'
$\Delta\delta^{13}$C$_{atm}$	-0.39‰	0‰
EEP $\Delta\delta^{13}$C	-0.41‰	-0.04‰
EEP $\Delta\delta^{13}$C$_{reg}$	-0.11‰	-0.09‰
EEP $\Delta\delta^{13}$C$_{pref}$	-0.3‰	+0.05‰

455
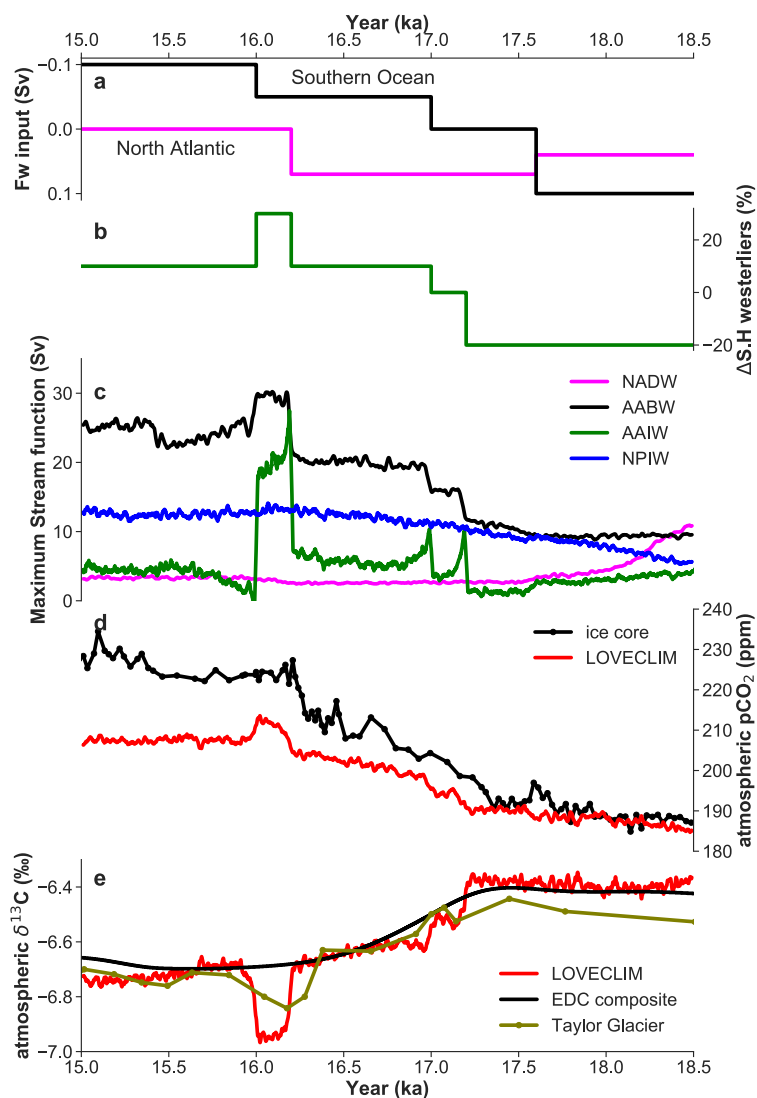
Figure 1. Timeseries from the LOVECLIM transient experiment (Menviel et al., 2018). a) Freshwater input into the North Atlantic and the Southern Ocean; b) Southern Hemisphere westerly wind forcing; c) simulated NADW, AABW, AAIW and NPIW maximum stream function in LOVECLIM. 21-year moving averages are shown for the maximum stream function to filter the high-frequency variability; d) ice core record of atmospheric CO_2 (Bereiter et al., 2015;

460 **Marcott et al., 2014) and LOVECLIM simulated atmospheric CO_2; e) atmospheric $\delta^{13}C$ records (Bauska et al., 2016; Schmitt et al., 2012) and LOVCLIM simulated atmospheric $\delta^{13}C$.**
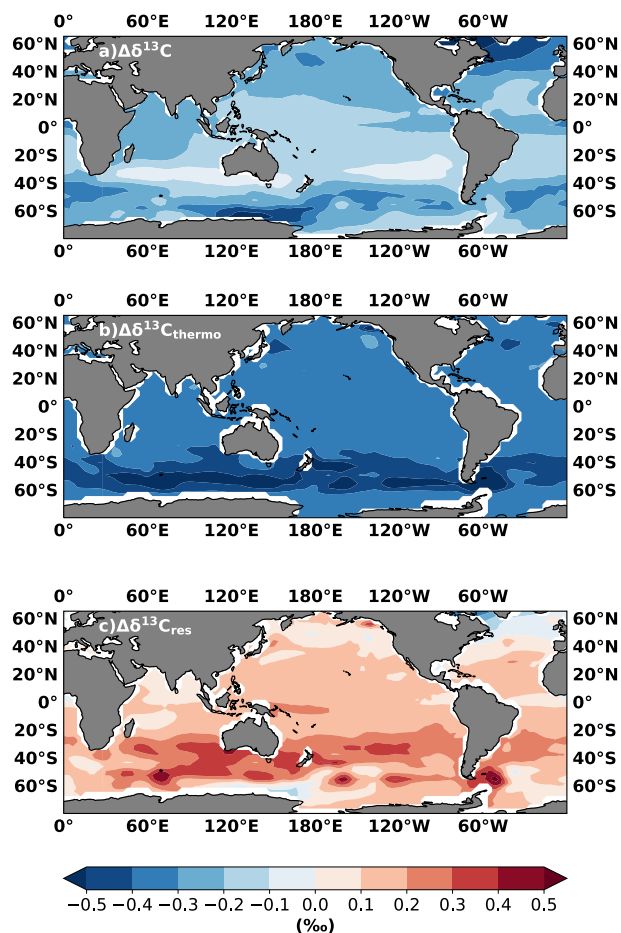
Figure 2. a) LOVECLIM simulated sea surface δ^{13}C anomaly (15-17.2 ka) b) sea surface δ^{13}C anomaly due to thermodynamic fractionation (air-sea exchange + SST effect) c) residual sea surface δ^{13}C anomaly that are not attributed to thermodynamic fractionation.
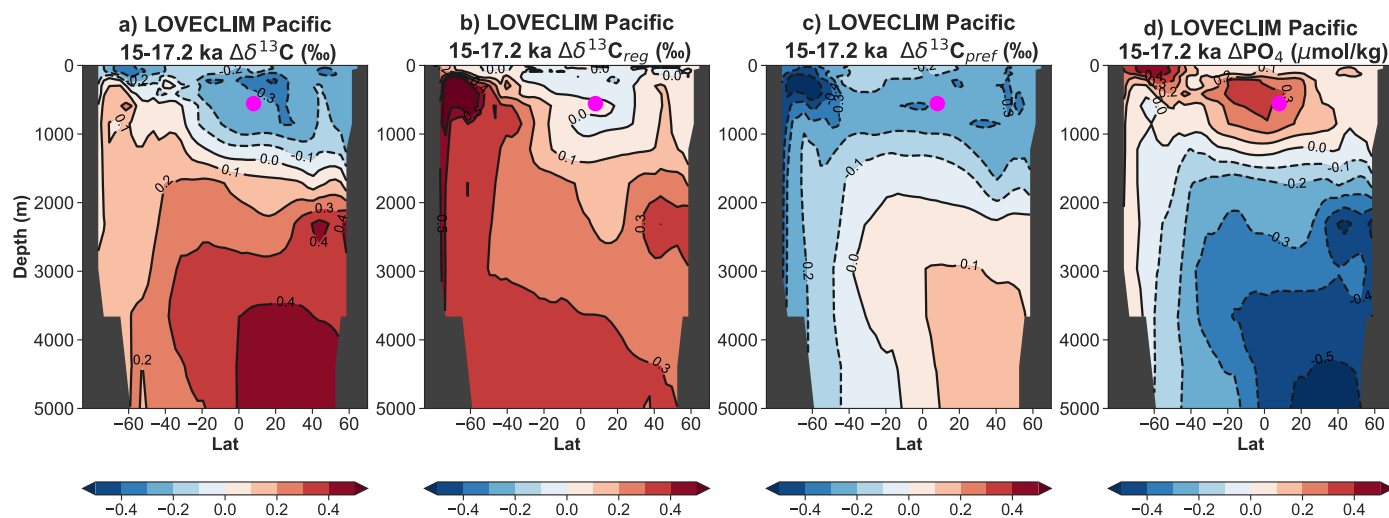
Figure 3. Pacific zonal averaged (160°E-140°W) a) δ^{13}C b) δ^{13}C$_{reg}$ c) δ^{13}C$_{pref}$ d) PO$_4$ anomaly (15ka minus 17.2ka) simulated by LOVECLIM. The magenta circle marks the GeoB17402 site.
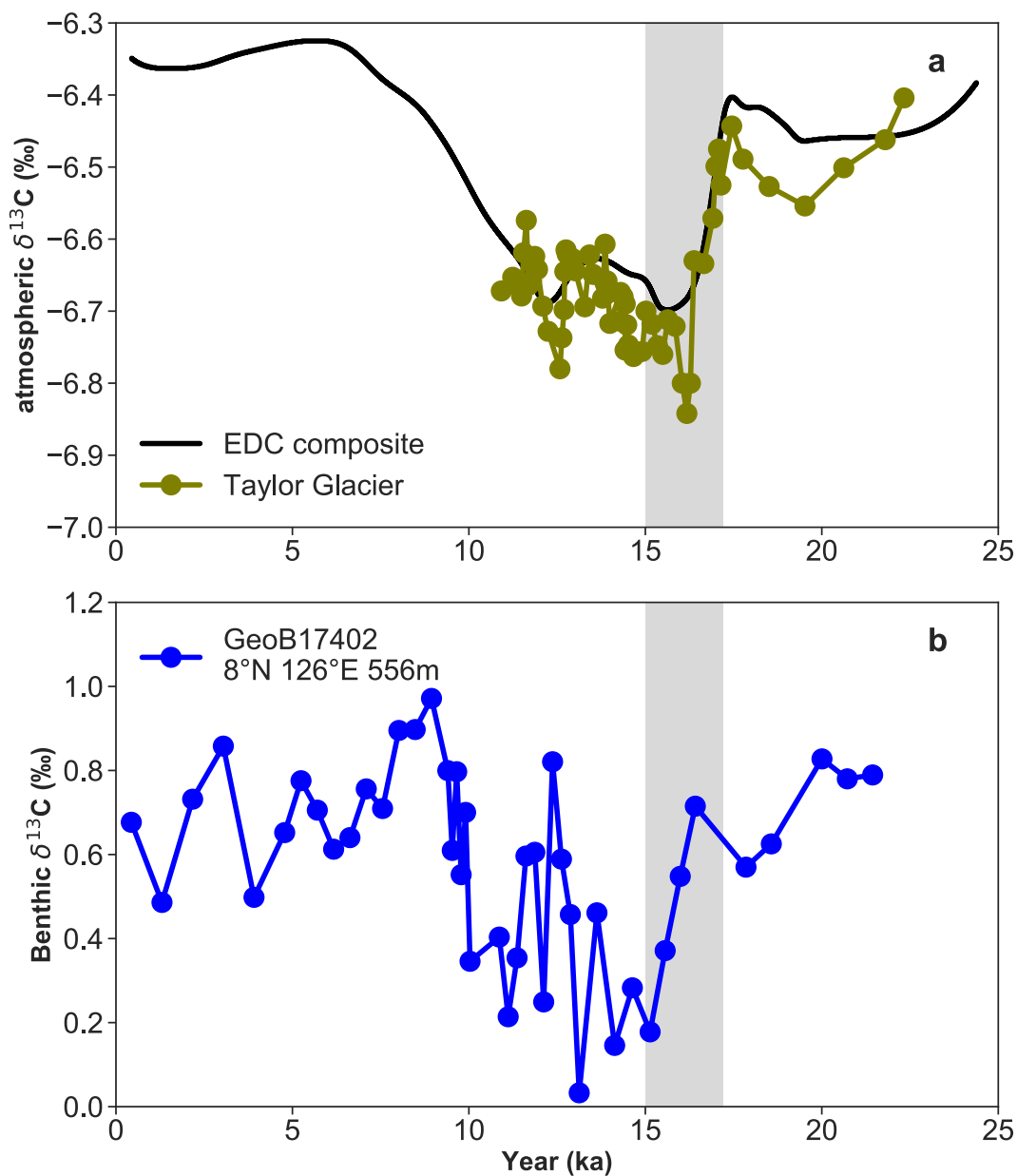
Figure 4. a): Atmospheric δ13C records (Bauska et al., 2016; Schmitt et al., 2012) b): *C. mundulus* **δ13C record for upper intermediate and mode waters in the western equatorial Pacific. The negative δ13C decline in the atmospheric and our benthic record are highlighted in a grey bar.**
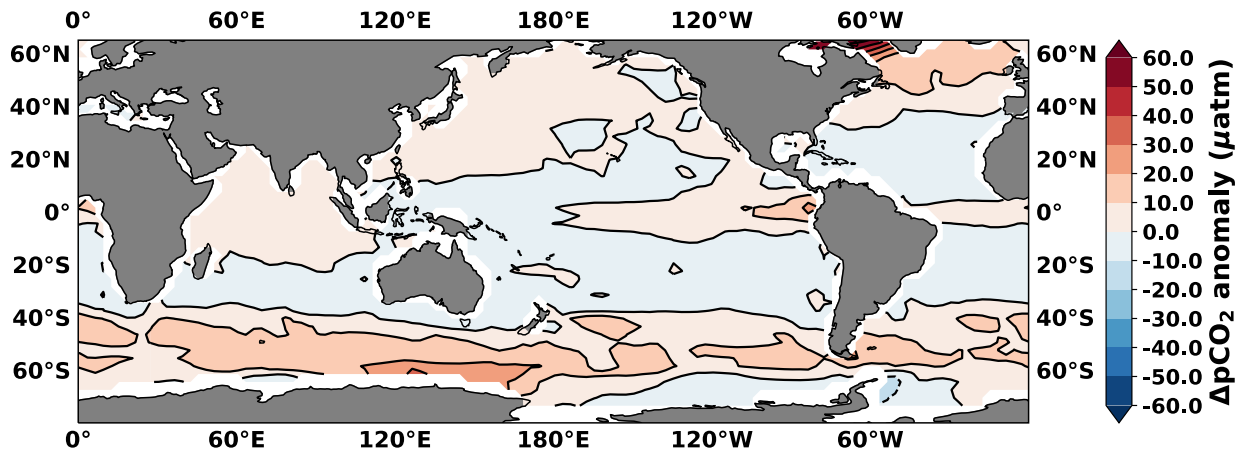
Figure 5. Changes in air-sea surface pCO$_2$ gradient (15-17.2 ka)
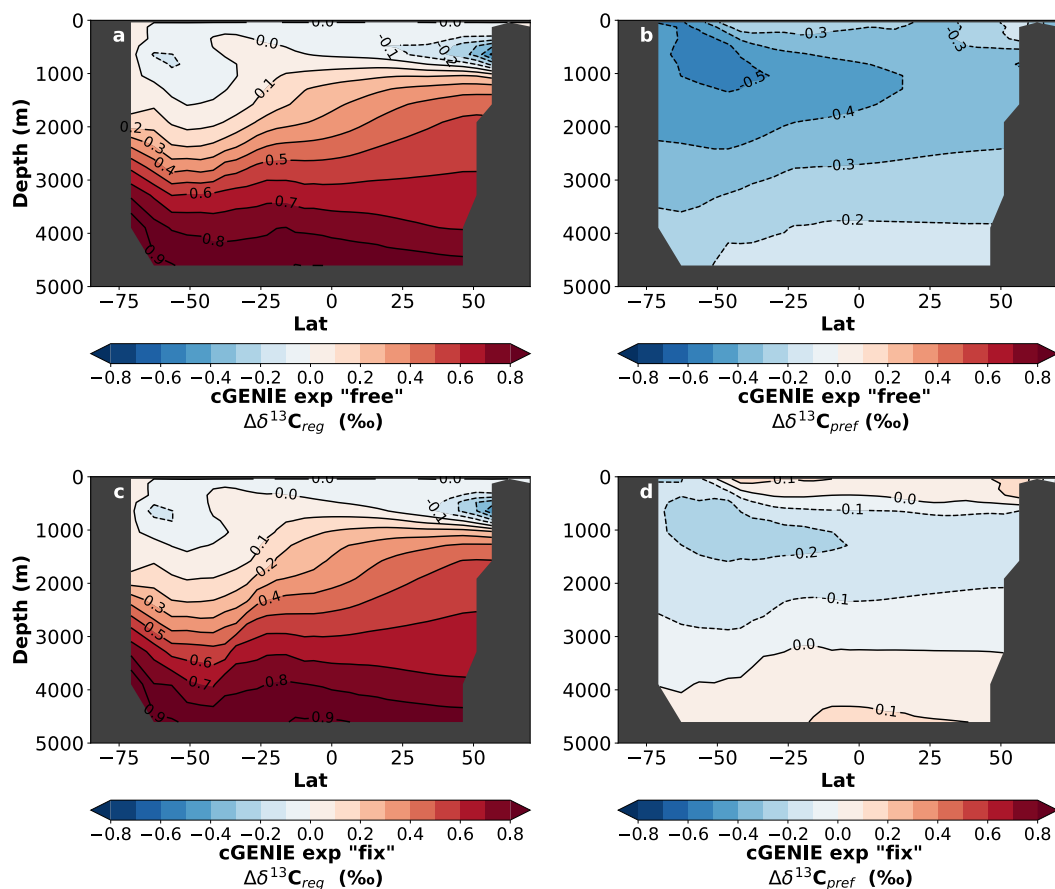
475

Figure 6. cGENIE simulated a) $\Delta\delta^{13}C_{reg}$ **b)** $\Delta\delta^{13}C_{pref}$ **in experiment 'free' and simulated c)** $\Delta\delta^{13}C_{reg}$ **d)** $\Delta\delta^{13}C_{pref}$ **in experiment 'fix'. Anomaly are calculated as the difference between model year 2000 and 0.**
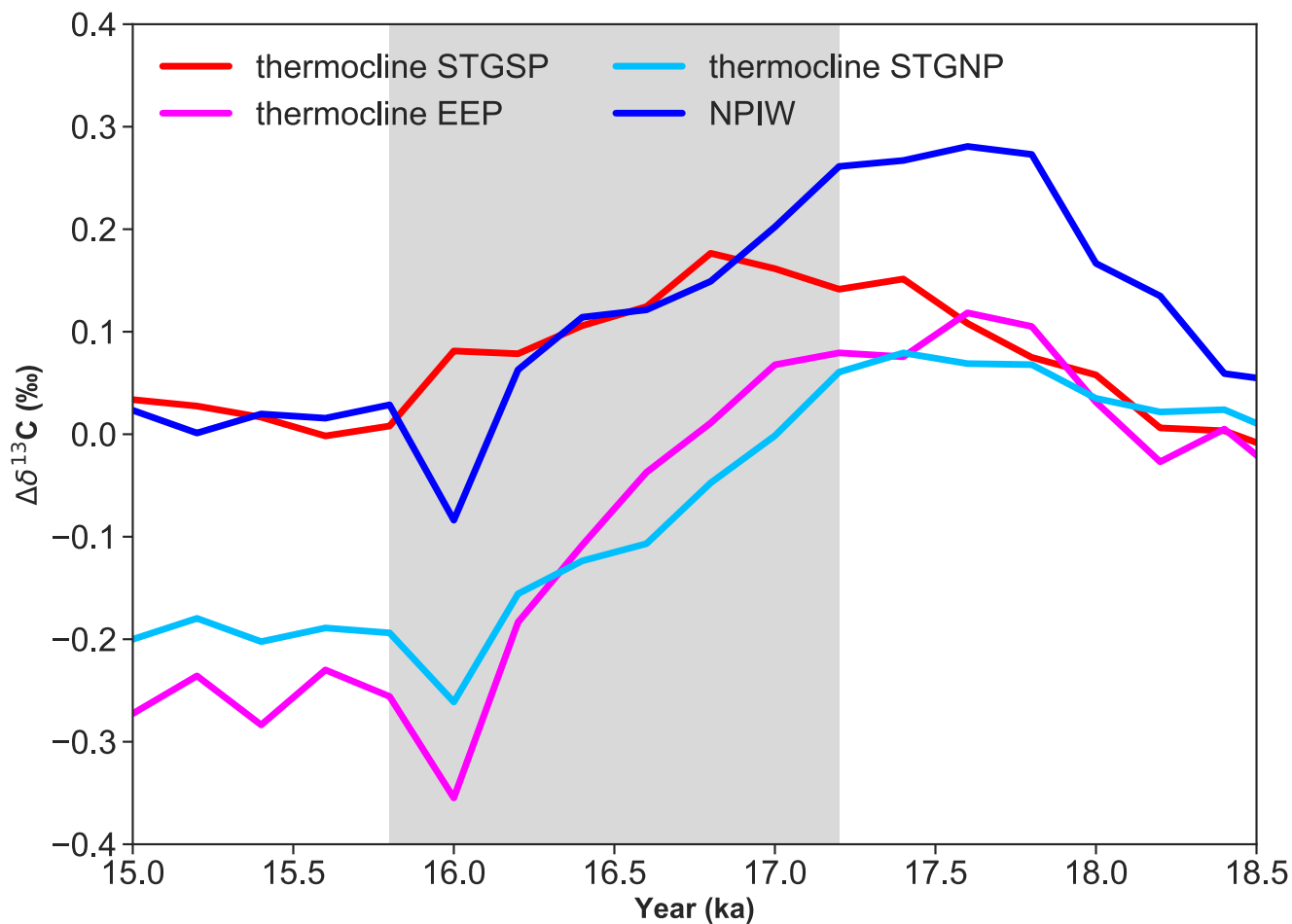
Figure 7. LOVECLIM simulated $\Delta\delta^{13}$C in thermocline EEP (90-82°W, 5°S-5°N, 77-105m), South Pacific subtropical

480 **gyre (STGSP, 160°E- 100°W, 40-22°S, 187-400m), North Pacific subtropical gyre (STGNP, 110°E- 140°W, 22-40°N,**

187-400m), NPIW (167-170°E, 54-57°N, 660m. The average of 23.8-20 ka (i.e. LGM) is used as a reference level for the

$\Delta\delta^{13}$C calculations. δ^{13}C decline between 17.2-15.8 ka is highlighted with a grey bar.
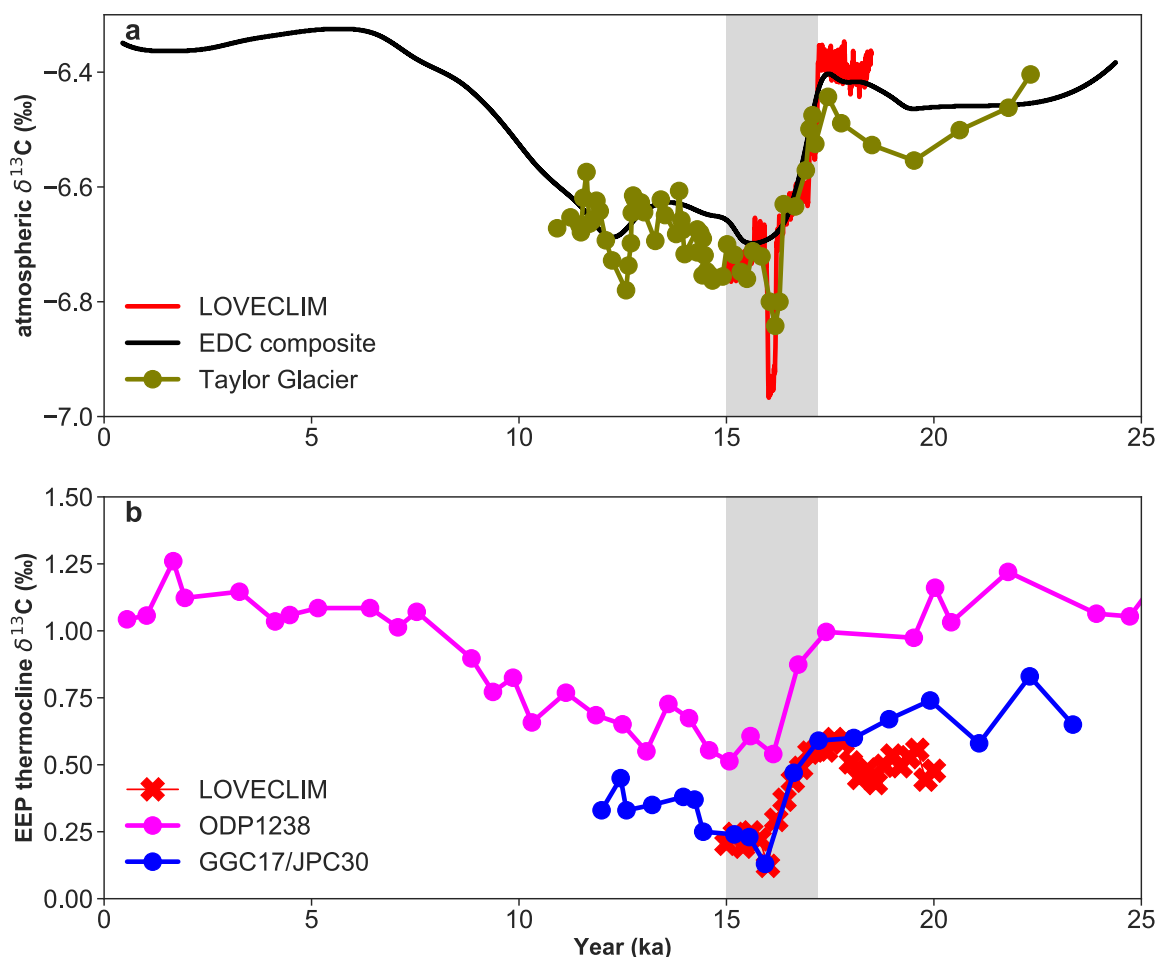
Figure 8. a): Atmospheric δ¹³C records (Bauska et al., 2016; Schmitt et al., 2012), simulated atmospheric δ¹³C (21-year

485 **running average) in LOVECLIM (Menviel et al., 2018) b):** *Neogloboquadrina. dutertrei* (*N. dutertrei*, **a shallow**

thermocline species) δ¹³C data from ODP 1238 (Martínez-Botí et al., 2015), GGC17/JPC30 (Zhao & Keigwin, 2018),

and LOVECLIM simulated δ¹³C of DIC at 100m (average of 82-90°W, 5°S-5°N). The *N. dutertrei* **data are corrected by**

-0.5‰ to normalize to δ¹³C of DIC (Spero et al., 2003). The grey shaded bars highlight the time period we focus in this

study.
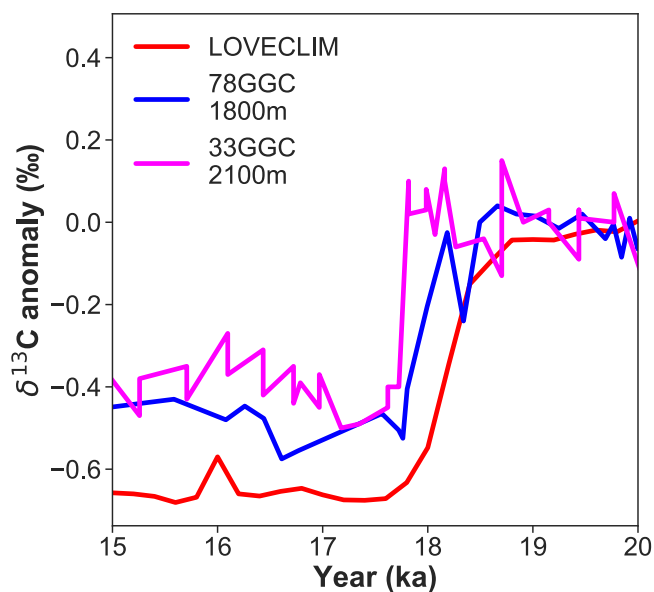
490

Figure 9. Observed δ^{13}C anomaly of 78GGC and 33GGC from the mid-depth of Brazil Margin at 27°S (Lund et al.,

2015) and simulated δ^{13}C anomaly at this location .
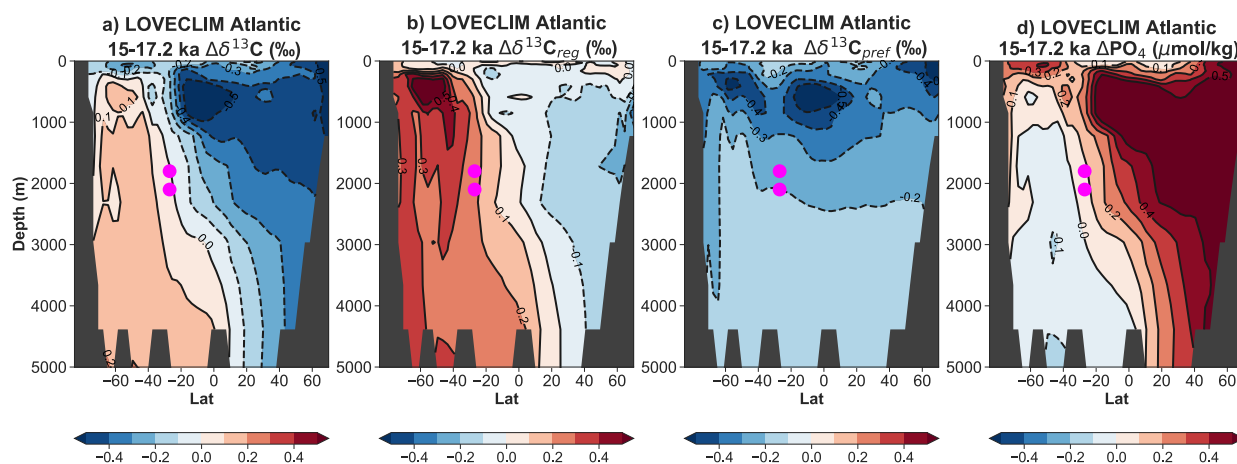
Figure 10. Same as Figure 3, but for the Atlantic zonal averaged (60°W-10°W) anomaly. The location of 78GGC and

495 **33GGC** (Lund et al., 2015) are marked as magenta circles.